Indian Journal of Pure & Applied Physics
Vol. 61, February 2023, pp. 102-107
DOI: 10.56042/ijpap.v61i2.69833

Temperature Dependence on Opto-structural Parameters of Sol-gel Derived Tin Doped Zirconia Nanoparticles

Saruchi Rani, Surbhi Verma & Sushil Kumar *
Department of Physics, Chaudhary Devi Lal University, Sirsa-125 055, Haryana, India

Received 23 December 2022; accepted 18 January 2023

Recently, nanocrystalline zirconia was widely employed in photocatalytic applications.Tin doped zirconia nanoparticles were prepared by sol-gel process followed by spin coating technique. The as-produced powders and thin films were heat treated in air at 500, 650 and 800 °C for 2h. Structural parameters of annealed samples were characterized by X-ray diffraction and Fourier transformed infrared studies. XRD spectra revealed the mixed phases such as t-ZrO_2, m-ZrO_2 and o-$ZrSnO_4$. Structural parameters viz. crystallite size, lattice constants, dislocation density, microstrain, orientation parameter and activation energy were evaluated. XRD data depicted that crystallite size increased, while lattice parameters slightly decreased with increase in annealing temperature. Expected functional groups were established by FTIR spectra. Optical parameters of nanopowders/thin films such as PL emission wavelength and optical band gap were determined by photoluminescence and UV-visible absorption. The energy band gaps of thin films were increased with increase in temperature. The emission peak exhibited a blue shift with increase in temperature. In addition, thermogravimetric-differential thermal analysis of as prepared sample was investigated.

Keywords: Nanoparicles; Sol-gel; Annealing; Structural parameters; Optical parameters

1 Introduction

Physico-chemical behaviour of metal oxides nanocomposites exhibits size dependence[1]. Nanocomposites have strength to enhance properties considerably of several nano and micro engineering systems e.g. gas sensors[2], liquid crystal displays, solar cells and solar collectors. Nanocomposite ZrO_2–SnO_2 possess significant technological values due to many opportunities such as tuning of bandgap, grain size, morphology etc. through the optimization of experimental conditions, minimize dislocations, and stress by preventing the propagation of faults, cracks etc. for utilization in optical as well as gas sensors[3]. Moreover, nano composites often depicted improved mechanical and thermal behaviour than that of their bulk copunterparts. Among different wide gap semiconductor nanoparticles, SnO_2 remained interesting because of its fantastic opto-electronic and electrical behaviour, as well as its sufficiently strong chemical stability[4]. Tin oxide (SnO_2) is n-type semiconductor[5] having energy bandgap E_g ~ 3.62–4.00 eV and possess diverse applications in solar cells, photovoltaic cells, liquid crystal displays, gas sensors, conducting electrodes, thin-film heaters and[6-9]. Zirconia (ZrO_2) is a versatile transition metal oxide having E_g ~ 5.5 eV employed in a wide range of applications e.g. oxygen and NO_x sensors, electrolytes of solid oxide fuel cells, ceramics. Preparation of advanced materials gifted with improved optical properties has increasingly pointed on nano-composite systems possessing complex stoichiometry as well as microstructures[10,11]. ZrO_2 is employed as an integral material in electro-optical devices and interference filters due to its optimum refractive index, wide energy gap, small optical losses and enormous transparency in VIS-NIR region[12]. Sol–gel followed by spin coating has been established as a popular means of producing composite nanoparticles and thin films. Through this approach structural and optical behaviour of prepared samples may be controlled easily by changing growth parameters viz. pH, concentration and temperature etc. of sol[13]. In addition, sol-gel is cost-effective route to produce homogeneous thin films at large scale. Although Anitha *et al.*[14] & Joy *et al.*[10] prepared thin films of SnO_2-ZrO_2 nanocomposites by sol-gel dip coating and analyzed them for their structural, optical and electrical properties but there are some more important parameters which needs to be still evaluated. In this communication, authors reported the fabrication of nanocrystalline ZrO_2–SnO_2 nanopowders/thin films using sol–gel route followed by spin coating, and investigated annealing effect on

*Corresponding authors: (E-mail: sushil.phys@gmail.com)

various structural and optical properties of prepared ZrO_2–SnO_2 nanocomposites.

2 Synthesis and Characterization

ZrO_2-SnO_2 nanopowders and thin films having molar ratio 0.85:0.15 were produced by sol-gel route followed by spin coating as shown in Fig. 1. The as-produced samples were assessed by techniques like X-ray diffraction, Fourier transform infrared spectroscopy, UV-visible absorption spectroscopy, photoluminescence and thermal analysis. XRD patterns of were obtained by X-ray diffractometer (Philips X'Pert PW3050) with CuK_α radiation (λ=1.5406Å) and 2θ 20-65^0. FTIR spectra were recorded in 4000-400 cm^{-1} with FTIR spectrometer (Perkin-Elmer 1600). PL spectra were saved in 400-550 nm using Fluorescence spectrometer (Perkin Elmer, LS-50B). UV-VIS absorption spectra were captured in 250–600 nm using UV-visible spectrophotometer (Comspec M550). Thermograms (TG-DTA) of as produced samples were recorded with thermal analyzer (Perkin Elmer, STA 6000).

3 Results and Discussion

3.1 XRD Studies

XRD spectra of ZrO_2-SnO_2 nanopowders heat treated at different temperatures are depicted in Fig. 2. The patterns exhibited the diffractions of monoclinic phase of ZrO_2 (m-ZrO_2) at 2θ ~ 24.3^0, 28.2^0 and 31.4^0 corresponding to planes (110), (111) and (200) [ICDD No. 37-1484]. Reflection peaks centered at about 2θ~30.3^0 (111), 35.3^0 (200), 50.2^0 (220) and 60.1^0 (111) planes have been observed and these reflections are corresponding to tetragonal phase of ZrO_2 (t-ZrO_2) [PDF no. 79-1769]. No significant phase of SnO_2 has been observed which may be due to low concentration and low ionic radii of tin precursor.

A peak confirming orthorhombic phase of $ZrSnO_4$ (o-$ZrSnO_4$) is situated at 2θ ~62.5^0. The evolution of o-$ZrSnO_4$ phase in sample upon crystallization is attributed to effective solubility of Sn^{4+} ions into the ZrO_2 lattice. ZrO_2–SnO_2 system exhibited the evolution of o-$ZrSnO_4$ phase in association with monoclinic ZrO_2 and tetragonal ZrO_2 phase at 500, 650 and 800 °C which are consistent with reported results[10,15]. The crystallite size with reference to most spectracular peak at ~28.11^0 (111) is calculated by Scherrer relation[16] and Williamson-Hall relation[17]:

$$D = \frac{k\lambda}{\beta \cos\theta}$$

$$\beta \cos\theta = \frac{k\lambda}{D} + \eta \sin\theta$$

where k is constant (0.94), λ is X-ray wavelength (1.5406Å), β is full width of spectral line at its half maxima, θ is angle of diffraction and η is micro-strain.

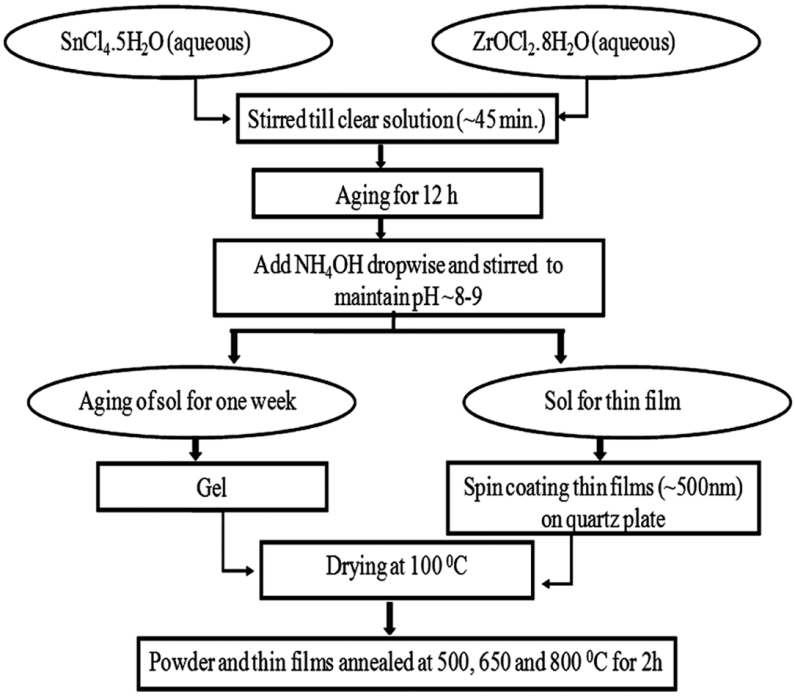

Fig. 1 — Flow chart for synthesis of sol-gel derived ZrO_2-SnO_2 system.

Table 1 — Structural parameters of ZrO_2-SnO_2 system

Temperature (°C)	Crystallite size D (nm)		Lattice constant		Unit cell volume V (Å^3)	Dislocation density δ (x 10^{3}nm^{-2})	Microstrain η
	D-S	W-H	a (Å)	c (Å)			
500	12.3	20.6	3.596	5.094	65.87	2.356	0.0074
650	19.6	28.9	3.585	5.086	65.32	1.197	0.0045
800	24.1	48.2	3.583	5.072	65.11	0.4304	0.0032

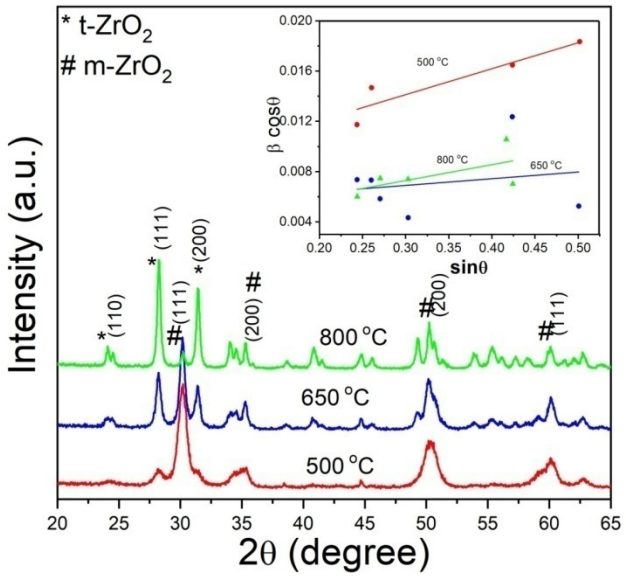

Fig. 2 — XRD patterns of ZrO_2-SnO_2 system annealed at different temperatures and inset shows the W-H plot for the same.

The dislocation density (δ) is given by the relation $\delta = 1/D^2$.

The calculated values of crystallite size, microstrain and dislocation density are depicted in Table 1. It has been seen that crystallite size rises, while microstrain and dislocation density diminish with annealing temperature.

The unit cell factors of the tetragonal phase of sample are determined as:

$$\frac{1}{d^2} = \frac{h^2 + k^2}{a^2} + \frac{l^2}{c^2}$$

$$V = a^2 c$$

where, d is plane spacing, a,b,c are lattice constants, h,k,l are Miller indices, and V is volume of unit cell. The cell factors of samples annealed at 800 °C are found to be c=5.072Å, a=3.583 Å and cell volume V= 65.11Å^3, which are consistent with the reported values in Ref.[18-19] and are given in Table 1.

The activation energy (ΔE) required to initiate a chemical reaction can be determined by Scott equation:

$$D = C \exp\left(\frac{-\Delta E}{RT}\right)$$

Table 2 — Orientation parameter $\gamma_{(hkl)}$ of ZrO_2-SnO_2 system

Temperature (°C)	Orientation parameter (γ)		
	(111)	(200)	(110)
500	0.117	0.143	0.203
650	0.308	0.310	0.295
800	0.576	0.547	0.502

Table 3 — Content of monoclinic phase in ZrO_2-SnO_2 system.

Content of monoclinc (%)	Temperature (°C)		
	500	650	800
For (111) plane	33%	59%	93%
For (200) plane	7%	34.2%	58%

where, D is crystallite size, C is pre-exponential factor, R is Rydberg constant, T is absolute temperature. A straight line is obtained on plotting log D vs. 1000/T as depicted in Fig. 3(d). The ΔE is assessed from the slope of straight line and is 9.46 KJ/mole.

The orientation parameter $\gamma_{(hkl)}$[20] is estimated from the relative heights of (111), (200), (110) diffraction peaks using following expression and are written in Table 2.

$$\gamma_{(hkl)} = \frac{I_{(hkl)}}{I_{(111)} + I_{(200)} + I_{(110)}}$$

The orientation parameter enhances with rise in annealing temperature.

The monoclinic content in samples consisting of both monoclinic and tetragonal phases is determined by peak intensity (I) according to following relation[21] and is shown in Table 3.

$$V_m = \frac{2.379\, I_{m(111)}}{I_{t(111)} + 2.379\, I_{m(111)}}$$

$$V_m = \frac{2.379\, I_{m(200)}}{I_{t(200)} + 2.379\, I_{m(200)}}$$

It has been found that monoclinic content in sample increases with temperature, which clearly exhibits that crystallites with monoclinic structure increases with the increase in temperature.

3.2 FTIR Studies

The main goal of FTIR analysis is to determine the chemical functional groups present in the sample.

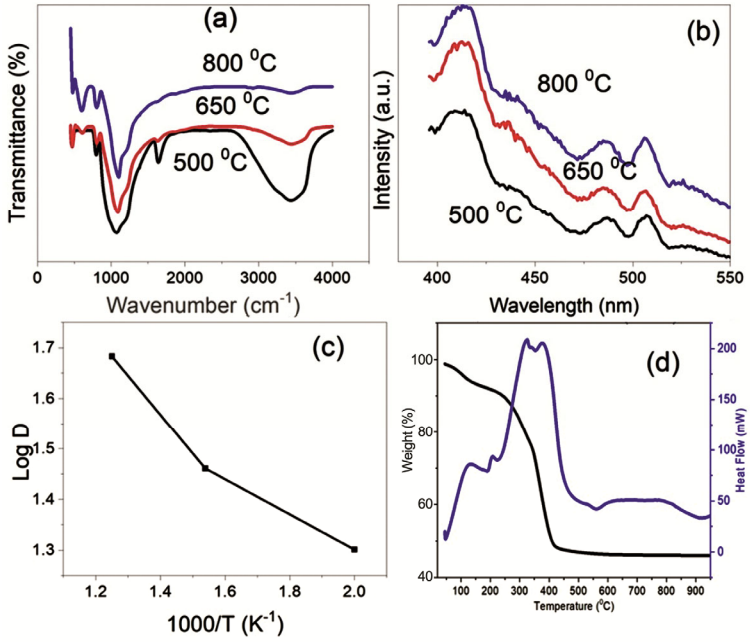

Fig. 3 — (a) FTIR spectra (b) PL spectra (c) TG-DTA curve (d) Graph plotted between log D and 1000/T for ZrO_2-SnO_2 system.

FTIR spectra of ZrO_2-SnO_2 system are shown in Fig. 3(a). A broad band seen at 3500 cm^{-1} attributed to -OH stretching vibration and an intense band at ~1625 cm^{-1} is because of H_2O bending vibration have been observed at 500 °C. Intensities of these band decreases on increasing annealing temperature and these bands completely disappeared at 800 °C.

The absorption bands at 1122, 1107 and 1091 cm^{-1} are attributed to bending vibration of hydroxyl groups present in zirconium oxide[22]. A characteristic peak of m-ZrO_2 at ~732 cm^{-1} starts developing and become stronger as annealing temperature is increased. The peak for metal oxygen bonding (Zr-O) is located at 582, 582 and 580 cm^{-1} corresponding to temperature 500, 650 and 800 °C respectively[23] and the peak at 497, 495 and 492 cm^{-1} have been observed corresponding to temperature 500, 650 and 800 °C respectively which may be due to Zr–O stretching in tetragonal ZrO_2[24,25]. These peaks are shifted towards lower wave number as temperature is increased from 650 to 800 °C and is due to Zr–O bond strengthening. With thermal treatment, the absorption due to OH groups is decreased and then disappeared while due to Zr–O–Zr increased. The results of FTIR are in agreement with that of XRD.

3.3 Photoluminescence Studies

Fig. 3 (a) — FTIR spectra (b) PL spectra (c) TG-DTA curve (d) Graph plotted between log D and 1000/T for ZrO_2-SnO_2 system.

The PL emission spectra of ZrO_2-SnO_2 system are shown in Fig. 3(b), which comprises peaks at 422, 484 and 510 nm. The peak at 422 nm can be caused by oxygen vacancies in $ZrSnO_4$, where oxygen interact with interstitial atoms of Zr and Sn, and attributed to form trapped states in band gap causing photoluminescence. The band at 484 nm can be attributed to oxygen vacancies present in SnO_2[10]. The band seen at 510 nm may be caused by mid-gap trapped states, i.e. surface defects.

It has been observed that, the emission bands decrease in intensity and shifted towards lower wavelength on increasing temperature. PL intensity varied with temperature as affected by crystallinity/defects of samples[25] and quenching mechanism due to OH groups[26]. It may be due to the fact that at low temperature, oxygen sub-lattice can have several defects, within the sample and at the surface[27]. Such defects are expected to possess non-radiative centers and therefore reduce light emission; while at high temperature, these non-radiative defects are reduced and re-structured resulting an enhancement in PL. The position of peak showed a blue shift from 422 to 410 nm, with rise in temperature. This blue shift is supposed to start off from change of stress in sample due to lattice distortion[27].

3.4 Thermal Analysis

Fig. 3(c) demonstrated the TG curve with a two-stage weight loss profile. In first stage, weight loss in

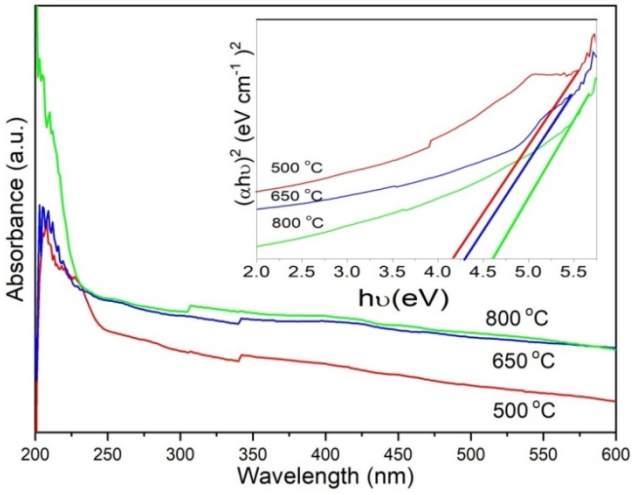

Fig. 4 — UV-visible absorption spectra and Tauc plot of ZrO_2-SnO_2 system annealed at different temperatures.

20-300 °C, is occurred as water is absorbed by precursors during hydrolysis. The exothermic peaks occurred at ~150 and 250 °C in DTA curve were due to evaporation of water and organic compounds. The second stage claimed a rapid weight loss in 300-400 °C, caused by the removal of organic compounds trapped in the network of gel. DTA plot displayed a broad exothermic peak between 310 and 400 °C, due to the crystallization of nanocomposites. Beyond 450 °C, thermogram did not exhibit any appreciable weight loss, and therefore the produced material may be treated as thermally stable material.

3.5 UV-visible Studies

The band gap of sample is estimated from Tauc's relation according to which absorption coefficient (α) is related to band gap (E_g) as[28]:

$$\alpha h\nu = A\left(h\nu - E_g\right)^n$$

where hυ is incident photon energy, and n is an index depending on electronic transition responsible for absorption process. The prepared system is of direct band gap in nature (n=1/2). To find band gap of prepared films, a graph (Tauc plot) was drawn between $(\alpha h\upsilon)^2$ and hυ which is shown in Fig. 4. The band gap of prepared films of nanocomposite ZrO_2-SnO_2 are found to be 4.15, 4.27 and 4.62 eV corresponding to 500, 650 and 800 °C respectively. The calculated band gap lies in between the band gap values for pure ZrO_2 (~5.1eV) and SnO_2 (~3.6 eV). It is noticed that band gap increases with annealing temperature which may be attributed to increased crystallinty of sample and is evident from XRD also.

4 Conclusions

ZrO_2-SnO_2 nanopowder/thin films were successively produced by sol-gel followed by spin coating. XRD spectra confirmed the existence of mixed phases such as t-ZrO_2, m-ZrO_2 and o-$ZrSnO_4$. XRD data demonstrated that crystallite size enhanced, while lattice parameters slightly reduced with increase in annealing temperature. The PL spectra revealed an emission peak at 422 nm in ZrO_2- SnO_2 system which depicted the existance of oxygen vacancies in $ZrSnO_4$. The band gap of ZrO_2–SnO_2 nanocomposite thin films was estimated as 4.15, 4.27 and 4.62 eV corresponding to 500, 650 and 800 °C respectively. These studies assessed that the produced material is its employable in optoelectronic devices.

References

1 Lakshmi J S, Berlin I J, Thomas J K, Thomas P V & Joy K, *IOP Conf Ser: Mater Sci Eng*, 23 (2011) 012030.
2 Korotcenkov G, *Sens Actuators B: Chem*, 107 (2005) 209.
3 Korotcenkov G, *Mater Sci Eng Rep*, 61 (2008) 1.
4 Kim T W, Kwak J K, Park K H, Yun D Y, Lee D U, Son D I & Lee J Y, *J Korean Phys Soc*, 57 (2010) 1803.
5 Lai M, Lim J H, Mubeen S, Rheem Y, Mulchandani A, Deshusses M A & Myung N V, *Nanotechnology*, 20 (2009) 185602.
6 Bhaktha B S, Kinowski C, Bouazaoui M, Capoen B, Robbe-Cristini O, Beclin F & Turrell S, *J Phys Chem C*, 113 (2009) 21555.
7 Patil G E, Kajale D D, Chavan D N, Pawar N K, Ahire P T, Shinde S D & Jain G H *Bullet Mater Sci*, 34 (2011) 1.
8 Ji Z, He Z, Song Y, Liu K & Ye Z, *J Cryst Growth*, 259 (2003) 282.
9 Mondal S P, Ray S K, Ravichandran J & Manna I, *Bullet Mater Sci*, 33 (2010) 357.
10 Joy K, Lakshmy S S & Thomas P V, *J Sol-gel Sci Technol*, 61 (2012)179.
11 Joy K, Lakshmy S S, Nair P B & Daniel G P, *J Alloys Compd*, 512 (2012) 149.
12 John B I, Lakshmi J S, Sujatha L S, Daniel G P, Thomas P V & Joy K, *J Sol-gel Sci Technol*, 58 (2011) 669.
13 Zhao Y, Wang T, Zhang D, Fan S, Shao J & Fan Z, *Appl Surf Sci*, 239 (2005)171.
14 Anitha V S, Lekshmy S S & Joy K, *J Mater Sci: Mater Electron*, 24 (2013) 4340.
15 Štefanić G, Musić S & Ivanda M, *Mater Res Bullet*, 43 (2008)2855.
16 Culity B & Stock S, Elements of X-ray Diffraction, Addition-Wesley, Reading, (1978).
17 Williamson G K & Hall W H, *Acta Metallurgica*, 1 (1953) 22.
18 Howard C J, Hill R J & Reichert B E, *Acta Crystal Sec B: Struct Sci*, 44 (1988)116.
19 Maniv S Westwood W D & Colombini E, *J Vacuum Sci Technol*, 20 (1982) 162.
20 Srivastava A, Shukla R K & Misra K P, *Cryst Res Technol*, 46 (2011) 949.
21 Wang Y H & Li X P, *Thin Solid Films*, 250 (1994) 132.

22 Zhang Y U, Yang M I N, Dou X M, He H & Wang D S, *Environ Sci Technol*, 39 (2005)7246.
23 Matos J M E, Júnior F A, Cavalcante L S, Santos V, Leal S H, Júnior L S & Longo, E, *Mater Chem Phys*, 117 (2009) 455.
24 Hirata T, Asari E & Kitajima M, *J Solid State Chem*, 110 (1994) 201.
25 Ortiz A, Alonso J C & Haro-Poniatowski E, *J Electron Mater*, 34 (2005) 150.
26 Yan Y, Faber A J & De Waal H, *J Non-Crystal Solids*, 181 (1995) 283.
27 Hong R, Huang J, He H, Fan Z & Shao J, *Appl Surf Sci*, 242 (2005) 346.
28 Zhang J & Gao L, *Mater Chem Phys*, 87 (2004) 10.